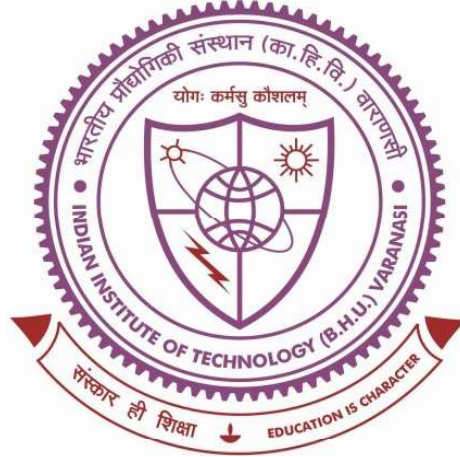


DEVELOPMENT OF BINARY, TERNARY, AND HIGH ENTROPY Ti ALLOYS FOR BIOMEDICAL IMPLANT APPLICATIONS



Thesis submitted in partial fulfillment for the
Award of Degree

Doctor of Philosophy

By

Rupesh Kumar

DEPARTMENT OF MECHANICAL ENGINEERING
INDIAN INSTITUTE OF TECHNOLOGY
(BANARAS HINDU UNIVERSITY)
VARANASI - 221005

Roll No. 19131502

2024



**INDIAN INSTITUTE OF TECHNOLOGY
(BANARAS HINDU UNIVERSITY) VARANASI
VARANASI-221005**

CERTIFICATE

It is certified that the work contained in the thesis titled **“DEVELOPMENT OF BINARY, TERNARY, AND HIGH ENTROPY Ti ALLOYS FOR BIOMEDICAL IMPLANT APPLICATIONS”** by **“RUPESH KUMAR”** has been carried out under my supervision and that this work has not been submitted elsewhere for a degree. A thesis submitted in partial fulfillment for the Award of Degree.

It is further certified that the student has fulfilled all the requirements of Comprehensive Examination, Candidacy, and SOTA for the award of Ph.D. Degree.

Prof. Rakesh Kumar Gautam

(Supervisor)

Dr. R.K. Gautam
Professor
Department of Mechanical Engineering
Mechanical Engineering Deptt.
Indian Institute of Technology (BHU)
Indian Institute of Technology (BHU)
Varanasi-221005, India Varanasi-221005 INDIA



INDIAN INSTITUTE OF TECHNOLOGY
(BANARAS HINDU UNIVERSITY) VARANASI
VARANASI-221005

DECLARATION BY THE CANDIDATE

I, “RUPESH KUMAR”, certify that the work embodied in this thesis is my own bonafide work and carried out by me under the supervision of “Prof. RAKESH KUMAR GAUTAM from “JANUARY 2020” to “DECEMBER 2024”, at the “Department of Mechanical Engineering”, Indian Institute of Technology (BHU), Varanasi, India. The matter embodied in this thesis has not been submitted for the award of any other degree/diploma. I declare that I have faithfully acknowledged and given credits to the research workers wherever their works have been cited in my work in this thesis. I further declare that I have not willfully copied any other’s work, paragraphs, text, data, results, *etc.*, reported in journals, books, magazines, reports dissertations, theses, *etc.*, or available at websites and have not included them in this thesis and have not cited as my own work.

Date:

Place: Varanasi

Rupesh Kumar
(RUPESH KUMAR)

CERTIFICATE BY THE SUPERVISOR

It is certified that the above statement made by the student is correct to the best of my knowledge.

Supervisor

(Prof. Rakesh Kumar Gautam)

IIT (BHU), Varanasi
India

Prof. R.K. Gautam
Professor
Mechanical Engineering Deptt.
Indian Institute of Technology (BHU)
Varanasi-221005 INDIA

Signature of Head of
Department

विभागाध्यक्ष/HEAD

यान्त्रिक अभियान्त्रिकी विभाग/Deptt. of Mechanical Engg.
भारतीय प्रौद्योगिकी संस्थान/Indian Institute of Technology
(का०हि०वि०/B.H.U.)

वाराणसी-221005/Varanasi-221005

COPYRIGHT TRANSFER CERTIFICATE

***Title of the Thesis:* DEVELOPMENT OF BINARY, TERNARY, AND HIGH ENTROPY Ti ALLOYS FOR BIOMEDICAL IMPLANT APPLICATIONS**

***Name of the Student:* Rupesh Kumar**

Copyright Transfer

The undersigned hereby assigns to the Indian Institute of Technology (Banaras Hindu University), Varanasi all rights under copyright that may exist in and for the above thesis submitted for the award of the **Doctor of Philosophy**.

Date:

Place:

Rupesh Kumar
(Rupesh Kumar)

Note: However, the author may reproduce or authorize others to reproduce material extracted verbatim from the thesis or derivative of the thesis for the author's personal use provided that the source and the Institute's copyright notice are indicated.

ACKNOWLEDGEMENT

The author is pleased to express his sincere thanks and gratitude beyond words to his supervisor Prof. Rakesh Kumar Gautam for their consistent help, encouragement, and valuable discussions during the entire period of his research work. The author would not have been able to complete the thesis without their utmost involvement and invaluable efforts. He motivated the author to pursue research problems and the need for persistent effort to accomplish the goal. The author is truly indebted to them.

Besides supervisors, the author would like to thank his RPEC and comprehensive members, Dr. U. S. Rao, Dr. A. K. Dubey, Dr. P. K. Roy, and Dr. D. Khan for their insightful comments and encouragement. The author acknowledges his deep sense of gratitude to the current and former Heads of the Department of Mechanical Engineering for providing all the research facilities to accomplish his research in the Department successfully. The author has an immense sense of gratitude to Prof. C. K. Behera and Prof. N. K. Mukhopadhyay (Department of Metallurgical Engineering, IIT BHU), Prof. M. R. Majhi (Department of Ceramic Engineering), Prof. Horesh Kumar (Department of Physics, BHU), Dr. Anita Mohan (Department of Physics, IIT BHU, Varanasi), Prof. Pralay Maiti (School of Materials Science and Technology, IIT BHU, Varanasi), and all the faculty members of the Department of Mechanical Engineering, IIT (BHU), Varanasi for their cooperation and inspiration.

The authors would like to extend their sincere gratitude to the Science and Engineering Research Board (SERB), a statutory body under the Department of Science and Technology (DST), Government of India, for their generous financial support, which was instrumental in carrying out this research work. The funding provided by SERB has facilitated the procurement of necessary materials, advanced equipment, and other

resources essential for the successful completion of this study.

The author is grateful to all his seniors Dr. Anurag Kumar Pandey, Dr. Homender Kumar, Dr. Asgar Shakil, Dr. Basudeb Rajak, Dr. Sudhakar Behera, Dr. Amod Kashyap, Dr. Suraj Singh Rawat, Dr. Manvender Singh, Dr. Arun Rajput, Dr. Ankit, Dr. Satyendra Kumar Singh, Dr. Pankaj Kumar Singh, Dr. Rakesh Ranjan Chand, Dr. Nitish Kumar, Dr. Nitish Kumar Mahto and friends Gulshan Verma, Mayank Singh, Kishor Kumar, Kartik Srivastava, Navnish Sonkar, Sankata Tiwari, Chitrance Srivastava, Gagan Bansal, Lalit Yadav, Anshu Raj, Vatsalya Raghuwanshi, Aditya Sharma, Ravi Ruwali, Raj Goyal, Devanand Gupta, Priyatosh Pradhan, Urvashi Kesharwani, Shrawanty Yadav,, Dilip Pathote, Vikrant Singh, Ashish Chouksey, and Pawan Ojha for their constant encouragement, making joyful and memorable life being with him in moments of happiness and difficulties at IIT (BHU), Varanasi. The author is also thankful to all CIF, workshop, lab, and office staff of the institute for their support.

The author would also like to express his immense gratitude to his parents, brothers, sisters, and relatives for their unconditional support and encouragement, to pursue his interest. The author also wishes to thank all those who have helped in any manner during the course of his research work.

The author would also like to express his immense gratitude to Bharat Ratna Mahamana Pandit Madan Mohan Malviya Ji for founding the beautiful campus of Banaras Hindu University. Finally, I extend my heartfelt gratitude to the holy city of Kashi, which embraced me and kept me healthy for such a long duration, enabling me to carry out this work.

RUPESH KUMAR

LIST OF FIGURES

Fig. No.	Captions	Page No.
Fig. 1.1	Schematic classification of biomedical implants	02
Fig. 1.2	Dental implant replacement	08
Fig. 1.3	Hip implant replacement	09
Fig. 1.4	Knee implant replacement	10
Fig. 1.5	Bone plates and screws	10
Fig. 2.1	Powder metallurgy flow chart	44
Fig. 3.1	XRD patterns of raw elemental powders	58
Fig. 3.2	SEM images of raw elemental powders (a) Ti (b) Nb (c) Zr (d) Mo (e) Cu (f) Sn	59
Fig. 3.3	Schematic diagram of Ti alloys processing through powder metallurgy technique	66
Fig. 3.4	Image of actual powder metallurgy processed samples	67
Fig. 3.5	Image of Bench top X-ray diffraction instrument	68
Fig. 3.6	Density measuring device based on Archimedes principle	69
Fig. 3.7	Vickers hardness tester	70
Fig. 3.8	Micro indentation test setup	71
Fig. 3.9	Corr test electrochemical potentiostat corrosion measuring device	73
Fig. 3.10	Bio-Tribometer test setup and schematic track formation	74
Fig. 3.11	Schematic diagram and image of the tribocorrosion test setup with a standard three-electrode system	76
Fig. 4.1	XRD patterns of binary Ti powder, Nb powder, and Ti-xNb milled powders	78
Fig. 4.2	XRD patterns of binary Ti powder, Zr powder, and Ti-xZr milled powders	79
Fig. 4.3	XRD patterns of binary Ti-10Zr and Ti-10Zr-xNb milled powders	80
Fig. 4.4	XRD pattern of TiNb _{1.5} Mo _{0.1} Zr _{1.15} Cu _{0.25} powder after milling	82
Fig. 4.5	XRD pattern of TiNbZr _{0.8} Mo _{0.92} Sn _{0.28} powder after milling	82
Fig. 4.6	XRD pattern of cpTi and Ti-6Al-4V	84
Fig. 4.7	XRD pattern of cpTi and sintered Ti-xNb alloys	85

Fig. 4.8	XRD pattern of sintered Ti-xZr alloys	85
Fig. 4.9	XRD pattern of sintered Ti-10Zr and Ti-10Zr-xNb alloys	86
Fig. 4.10	XRD pattern of sintered TiNb _{1.5} Mo _{1.1} Zr _{1.15} Cu _{0.25} HEA	88
Fig. 4.11	XRD pattern of sintered TiNbZr _{0.8} Mo _{0.92} Sn _{0.28} HEA	88
Fig. 4.12	SEM images of cpTi and Ti-6Al-4V	89
Fig. 4.13	SEM images of (a) cpTi, (b) Ti-5Nb, (c) Ti-10Nb, (d) Ti-15Nb, (e) Ti-20Nb, and (f) Ti-25Nb sintered alloys	91
Fig. 4.14	Elemental mapping of (a) Ti-5Nb, (b) Ti-10Nb, (c) Ti-15Nb, (d) Ti-20Nb, and (e) Ti-25Nb sintered alloys	92
Fig. 4.15	SEM images of (a) Ti-5Zr, (c) Ti-10Zr, (d) Ti-15Zr, (e) Ti-20Zr, and (f) Ti-25Zr sintered alloys	93
Fig. 4.16	Elemental mapping of (a) Ti-5Zr, (b) Ti-10Zr, (c) Ti-15Zr, (d) Ti-20Zr, and (e) Ti-25Zr sintered alloys	94
Fig. 4.17	SEM images of sintered ternary (a)Ti-10Zr-5Nb, (b) Ti-10Zr-10Nb, (c) Ti-10Zr-15Nb, (d) Ti-10Zr-20Nb alloys	96
Fig. 4.18	Elemental mapping of sintered ternary (a)Ti-10Zr-5Nb, (b) Ti-10Zr-10Nb, (c) Ti-10Zr-15Nb, (d) Ti-10Zr-20Nb alloys	97
Fig. 4.19	SEM images of (a) sintered TiNb _{1.5} Mo _{1.1} Zr _{1.15} Cu _{0.25} at 5000x, (b) sintered TiNb _{1.5} Mo _{1.1} Zr _{1.15} Cu _{0.25} at 10000x, (c) sintered TiNbZr _{0.8} Mo _{0.92} Sn _{0.28} at 5000x, (d) sintered TiNbZr _{0.8} Mo _{0.92} Sn _{0.28} at 10000x	99
Fig. 4.20	Elemental mapping image of (a) sintered TiNb _{1.5} Mo _{1.1} Zr _{1.15} Cu _{0.25} and (a1-a5) corresponding elemental distribution (b) sintered TiNb _{1.5} Mo _{1.1} Zr _{1.15} Cu _{0.25} and (b1-b5) corresponding elemental distribution	100
Fig. 4.21	Vickers hardness of cpTi and Ti-6Al-4V alloy	105
Fig. 4.22	Vickers hardness of sintered Ti-xNb alloys	107
Fig. 4.23	Vickers hardness of sintered Ti-xZr alloys	107
Fig. 4.24	Vickers hardness of sintered Ti-10Zr-xNb alloys	108
Fig. 4.25	Vickers hardness of sintered TiNb _{1.5} Mo _{1.1} Zr _{1.15} Cu _{0.25} and TiNbZr _{0.8} Mo _{0.92} Sn _{0.28} high entropy alloys	109

Fig. 4.26	Load displacement curve obtained for cpTi and Ti-6Al-4V from micro indentation testing	110
Fig. 4.27	Load displacement curve obtained for binary Ti-xNb alloys from micro indentation testing	111
Fig. 4.28	Load displacement curve obtained for binary Ti-xZr alloys from micro indentation testing	113
Fig. 4.29	Load displacement curve obtained for ternary Ti-10Zr-xNb alloys from micro indentation testing	114
Fig. 4.30	Load displacement curve obtained for TiNb _{1.5} Mo _{1.1} Zr _{1.15} Cu _{0.25} and TiNbZr _{0.8} Mo _{0.92} Sn _{0.28} high entropy alloys from micro indentation testing	115
Fig. 5.1	Corrosion response of cpTi and Ti-6Al-4V (a) Nyquist plot, (b) Bode plot, (c) Tafel plot, and (d) Equivalent circuit diagram	121
Fig. 5.2	Corrosion response of Ti-xNb alloys (a) Nyquist plot, (b) Bode plot, (c) Tafel plot, and (d) Equivalent circuit diagram	127
Fig. 5.3	Corrosion response of Ti-xZr alloys (a) Nyquist plot, (b) Bode plot, (c) Tafel plot, and (d) Equivalent circuit diagram	129
Fig. 5.4	Corrosion response of Ti-10Zr-xNb alloys (a) Nyquist plot, (b) Bode plot, (c) Tafel plot, and (d) Equivalent circuit diagram	132
Fig. 5.5	Corrosion response of high entropy alloys (a) Nyquist plot, (b) Bode plot, (c) Tafel plot, and (d) Equivalent circuit diagram	134
Fig. 5.6	SEM images of corroded surface of (a) cpTi and (b) Ti-6Al-4V	136
Fig. 5.7	SEM images and EDS analysis of corroded surface of (a) Ti-5Nb, (b) Ti-10Nb, (c) Ti-15Nb, (d) Ti-20Nb, and (e) Ti-25Nb alloys.	138
Fig. 5.8	SEM images and EDS analysis of corroded surface of (a) Ti-5Zr, (b) Ti-10Zr, (c) Ti-15Zr, and (d) Ti-20Zr alloys.	140
Fig. 5.9	SEM images and EDS analysis of corroded surface of (a) Ti-10Zr-5Nb, (b) Ti-10Zr-10Nb, (c) Ti-10Zr-15Nb, and (d) Ti-10Zr-20Nb alloys.	142
Fig. 5.10	SEM images and EDS analysis of corroded surface of (a)	143

	sintered $\text{TiNb}_{1.5}\text{Mo}_{1.1}\text{Zr}_{1.15}\text{Cu}_{0.25}$ HEA, (b) sintered $\text{TiNbZr}_{0.8}\text{Mo}_{0.92}\text{Sn}_{0.28}$ HEA	
Fig. 5.11	Coefficient of friction response for (a) cpTi, (b) Ti-6Al-4V, (c) average friction coefficient of cpTi and Ti-6Al-4V	144
Fig. 5.12	Coefficient of friction of Ti-xNb alloys in SBF (a) Ti-5Nb, (b) Ti-10Nb, (c) Ti-15Nb, (d) Ti-20Nb, (e) Ti-25Nb, and (f) Average COF response	146
Fig. 5.13	Coefficient of friction of Ti-xZr alloys in SBF (a) Ti-5Zr, (b) Ti-10Zr, (c) Ti-15Zr, (d) Ti-20Zr, (e) Ti-25Zr, and (f) Average COF response	147
Fig. 5.14	Coefficient of friction of Ti-10Zr-xNb alloys in SBF (a) Ti-10Zr-5Nb, (b) Ti-10Zr-10Nb, (c) Ti-10Zr-15Nb, (d) Ti-10Zr-20Nb, (e) Average COF response	148
Fig. 5.15	COF vs Cycle graph of (a) $\text{TiNb}_{1.5}\text{Mo}_{1.1}\text{Zr}_{1.15}\text{Cu}_{0.25}$ HEA, (b) $\text{TiNbZr}_{0.8}\text{Mo}_{0.92}\text{Sn}_{0.28}$ HEA, (c) Average COF response	149
Fig. 5.16	Wear track profile of cpTi at 10, 20, 30, and 40 N loads	150
Fig. 5.17	Wear track profile of Ti-6Al-4V at 10, 20, 30, and 40 N loads	151
Fig. 5.18	Wear track profile of Ti-xNb alloys at 10 N	154
Fig. 5.19	Wear track profile of Ti-xNb alloys at 20 N	155
Fig. 5.20	Wear track profile of Ti-xNb alloys at 30 N	156
Fig. 5.21	Wear track profile of Ti-xNb alloys at 40 N	157
Fig. 5.22	Wear track profile of Ti-xZr alloys at 10 N	158
Fig. 5.23	Wear track profile of Ti-xZr alloys at 20 N	159
Fig. 5.24	Wear track profile of Ti-xZr alloys at 30 N	160
Fig. 5.25	Wear track profile of Ti-xZr alloys at 40 N	161
Fig. 5.26	Wear track profile of Ti-10Zr-xNb alloys at 20 N	162
Fig. 5.27	Wear track profile of Ti-10Zr-xNb alloys at 30 N	163
Fig. 5.28	Wear track profile of Ti-10Zr-xNb alloys at 40 N	163
Fig. 5.29	Wear track profile of sintered HEA Cu at 20 and 30 N	165
Fig. 5.30	Wear track profile of sintered HEA Sn at 20 and 30 N	166
Fig. 5.31	SEM images of worn surfaces of cpTi and Ti-6Al-4V at (a)10 N, (b) 20 N, (c) 30 N, and (d) 40 N, with corresponding (a ₁ , b ₁ , c ₁ , d ₁) at higher magnification	169

Fig. 5.32	SEM images of worn surfaces of Ti-xNb alloys at 10 and 20 N	170
Fig. 5.33	SEM images of worn surfaces of Ti-xNb alloys at 30 and 40 N	171
Fig. 5.34	EDS spectra of worn surfaces of Ti-xNb alloys at 10 N	172
Fig. 5.35	SEM images of worn surfaces of Ti-xZr alloys at 10 and 20 N	173
Fig. 5.36	SEM images of worn surfaces of Ti-xZr alloys at 30 and 40 N	174
Fig. 5.37	EDS spectra of worn surfaces of Ti-xZr alloys at 10 N	175
Fig. 5.38	SEM images of worn surfaces of Ti-10Zr-xNb alloys at 20 N	176
Fig. 5.39	SEM images of worn surfaces of Ti-10Zr-xNb alloys at 30 and 40 N	177
Fig. 5.40	EDS spectra of worn surfaces of Ti-10Zr-xNb alloys at 20 N	178
Fig. 5.41	SEM micrograph after wear of A) $\text{TiNb}_{1.5}\text{Mo}_{0.1}\text{Zr}_{1.15}\text{Cu}_{0.25}$ at 20N 150x, B) $\text{TiNb}_{1.5}\text{Mo}_{0.1}\text{Zr}_{1.15}\text{Cu}_{0.25}$ at 30N 150x, C) $\text{TiNbZr}_{0.8}\text{Mo}_{0.92}\text{Sn}_{0.28}$ at 20N 150x, D) $\text{TiNbZr}_{0.8}\text{Mo}_{0.92}\text{Sn}_{0.28}$ at 30N 150x, E) $\text{TiNb}_{1.5}\text{Mo}_{0.1}\text{Zr}_{1.15}\text{Cu}_{0.25}$ at 1000x, F) $\text{TiNbZr}_{0.8}\text{Mo}_{0.92}\text{Sn}_{0.28}$ at 1000x	179
Fig. 6.1	Tribocorrosion response of cpTi and Ti-6Al-4V (a) OCP test, (b) PDP test	184
Fig. 6.2	Wear track profile after tribocorrosion test of cpTi and Ti-6Al-4V for OCP and PDP test	185
Fig. 6.3	Tribocorrosion response of binary Ti-xNb alloys (a) OCP test, (b) PDP test	188
Fig. 6.4	Tribocorrosion response of binary Ti-xZr alloys (a) OCP test, (b) PDP test	188
Fig. 6.5	Wear track profile after tribocorrosion test of Ti-xNb alloys for OCP and PDP test	189
Fig. 6.6	Wear track profile after tribocorrosion test of Ti-xZr alloys for OCP and PDP test	190
Fig. 6.7	Tribocorrosion response of ternary Ti-10Zr-xNb alloys (a) OCP test, (b) PDP test	193
Fig. 6.8	Wear track profile after tribocorrosion test of Ti-10Zr-xNb alloys for OCP and PDP test	194

Fig. 6.9	Tribocorrosion response of high entropy alloys (a) OCP test, (b) PDP test	196
Fig. 6.10	Wear track profile after tribocorrosion test of high entropy alloys for OCP and PDP test of HEAs	196
Fig. 6.11	Worn surfaces of (a) cpTi, (b) Ti-6Al-4V after OCP, and corresponding (a ₁ -b ₁) for PDP tribocorrosion test	201
Fig. 6.12	Worn surfaces of (a) Ti-5Nb, (b) Ti-10Nb, (c) Ti-15Nb, (d) Ti-20Nb, (e) Ti-25Nb after OCP, and corresponding (a ₁ -e ₁) for PDP tribocorrosion test	202
Fig. 6.13	Worn surfaces of (a) Ti-5Zr, (b) Ti-10Zr, (c) Ti-15Zr, (d) Ti-20Zr, (e) Ti-25Zr after OCP, and corresponding (a ₁ -e ₁) for PDP tribocorrosion test	203
Fig. 6.14	Worn surfaces of (a) Ti-10Zr-5Nb, (b) Ti-10Zr-10Nb, (c) Ti-10Zr-15Nb, (d) Ti-10Zr-20Nb after OCP, and corresponding (a ₁ -d ₁) for PDP tribocorrosion test	204
Fig. 6.15	Worn surfaces of (a) TiNb _{1.5} Mo _{1.1} Zr _{1.15} Cu _{0.25} , (b) TiNbZr _{0.8} Mo _{0.92} Sn _{0.28} after OCP, and corresponding (a ₁ -b ₁) for PDP tribocorrosion test	205

LIST OF TABLES

Table No.	Captions	Page No.
Table 2.1	Conventional metallic materials and their mechanical, biological, tribological, and corrosion response	23
Table 2.2	Binary Ti alloys and their mechanical properties	30
Table 2.3	Ternary Ti alloys and their mechanical properties	35
Table 2.4	High entropy Ti alloys and their mechanical properties	41
Table 3.1	Details of elemental raw material used for development of the alloys	58
Table 3.2	Atomic percentage, atomic radius, and VEC of various elements in TiNb _{1.5} Mo _{0.1} Zr _{1.15} Cu _{0.25} HEA	63
Table 3.3	Enthalpy of mixing of binary alloys (ΔH_{ij}^{mix} , kJ/mol) for TiNb _{1.5} Mo _{0.1} Zr _{1.15} Cu _{0.25} HEA, following Miedema's approach	63
Table 3.4	Atomic percentage, atomic radius, and VEC of various elements in TiNbZr _{0.8} Mo _{0.92} Sn _{0.28} HEA	64
Table 3.5	Enthalpy of mixing of binary alloys (ΔH_{ij}^{mix} , kJ/mol) for TiNbZr _{0.8} Mo _{0.92} Sn _{0.28} HEA, following Miedema's approach	64
Table 3.6	Design parameters of TiNb _{1.5} Mo _{0.1} Zr _{1.15} Cu _{0.25} and TiNbZr _{0.8} Mo _{0.92} Sn _{0.28} HEAs	65
Table 3.7	Constituents and their quantity of simulated body fluid solution	72
Table 4.1	Theoretical and actual density of cpTi and Ti-6Al-4V alloy	101
Table 4.2	Theoretical density, sintered density, and percentage porosity of Ti-Nb alloys	102
Table 4.3	Theoretical density, sintered density and percentage porosity of Ti-Zr alloys	102
Table 4.4	Theoretical density, sintered density and percentage porosity of Ti-10Zr-xNb alloys	103
Table 4.5	Theoretical density, sintered density and percentage	104

	porosity of HEAs	
Table 4.6	Elastic modulus of cpTi and Ti-6Al-4V alloy	110
Table 4.7	Elastic modulus of sintered Ti-xNb alloys	112
Table 4.8	Elastic modulus of sintered Ti-xZr alloys	113
Table 4.9	Elastic modulus of sintered Ti-10Zr-xNb alloys	114
Table 4.10	Elastic modulus of TiNb _{1.5} Mo _{1.1} Zr _{1.15} Cu _{0.25} and TiNbZr _{0.8} Mo _{0.92} Sn _{0.28} high entropy alloys	115
Table 5.1	Impedance parameters derived from EIS fitting for cpTi and Ti-6Al-4V alloys	121
Table 5.2	Corrosion parameters obtained from Tafel extrapolation for cpTi and Ti-6Al-4V alloys	122
Table 5.3	Impedance parameters derived from EIS fitting for Ti-xNb alloys	128
Table 5.4	Corrosion parameters obtained from Tafel extrapolation for Ti-xNb alloys	128
Table 5.5	Impedance parameters derived from EIS fitting for Ti-xZr alloys	129
Table 5.6	Corrosion parameters obtained from Tafel extrapolation for Ti-xZr alloys	130
Table 5.7	Impedance parameters derived from EIS fitting for Ti-10Zr-xNb alloys	132
Table 5.8	Corrosion parameters obtained from Tafel extrapolation for Ti-10Zr-xNb alloys	133
Table 5.9	Impedance parameters derived from EIS fitting for high entropy alloys	135
Table 5.10	Corrosion parameters obtained from Tafel extrapolation for high entropy alloys	135
Table 5.11	Wear scar parameters, wear volume, and wear rates of cpTi at 10, 20, 30, and 40 N in SBF condition	151
Table 5.12	Wear scar parameters, wear volume, and wear rates of Ti-	152

	6Al-4V at 10, 20, 30, and 40 N in SBF condition	
Table 5.13	Wear scar parameters, wear volume, and wear rates of Ti-xNb alloys at 10 N in SBF condition	154
Table 5.14	Wear scar parameters, wear volume, and wear rates of Ti-xNb alloys at 20 N load in SBF condition	155
Table 5.15	Wear scar parameters, wear volume, and wear rates of Ti-xNb alloys at 30 N load in SBF condition	156
Table 5.16	Wear scar parameters, wear volume, and wear rates of Ti-xNb alloys at 40 N load in SBF condition	157
Table 5.17	Cross-sectional area, average wear depth, width of wear scar, wear rate and wear volume of Ti-xZr alloys at 10 N.	158
Table 5.18	Cross-sectional area, average wear depth, width of wear scar, wear rate and wear volume of Ti-xZr alloys at 20 N	159
Table 5.19	Cross-sectional area, average wear depth, width of wear scar, wear rate and wear volume of Ti-xZr alloys at 30 N	160
Table 5.20	Cross-sectional area, average wear depth, width of wear scar, wear rate and wear volume of Ti-xZr alloys at 40 N	161
Table 5.21	Wear parameter of ternary Ti-10Zr-xNb at 20N	164
Table 5.22	Wear parameter of ternary Ti-10Zr-xNb at 30N	164
Table 5.23	Wear parameter of ternary Ti-10Zr-xNb at 40N	164
Table 5.24	Calculated wear volume and wear rate of sintered HEA Cu at 20 and 30 N	165
Table 5.25	Calculated wear volume and wear rate of sintered HEA Sn at 20 and 30 N	166
Table 6.1	Wear parameters resulting from tribo-corrosion test in OCP and PDP test for cpTi and Ti-6Al-4V	185
Table 6.2	Wear parameters resulting from tribo-corrosion test in OCP test of Ti-xNb alloys	191
Table 6.3	Wear parameters resulting from tribo-corrosion test in PDP test of Ti-xNb alloys	191
Table 6.4	Wear parameters resulting from tribo-corrosion test in OCP test of Ti-xZr alloys	192

Table 6.5	Wear parameters resulting from tribo-corrosion test in PDP test of Ti-xZr alloys	192
Table 6.6	Wear parameters resulting from tribo-corrosion test in OCP test of Ti-10Zr-xNb alloys	195
Table 6.7	Wear parameters resulting from tribo-corrosion test in PDP test of Ti-10Zr-xNb alloys	195
Table 6.8	Wear parameters resulting from tribo-corrosion test in OCP and PDP test of high entropy alloys	197
Table 6.9	Wear parameters resulting from tribo-corrosion test in OCP and PDP test of high entropy alloys	197

LIST OF ABBREVIATIONS & SYMBOLS

SS 316	:	Low carbon stainless steel
Co-Cr	:	Cobalt-Chromium
Ni	:	Nickel
cpTi	:	Commercially pure titanium
HCP	:	Hexagonal closed packed
BCC	:	Body centered cubic
mm	:	Millimeter
XRD	:	X-Ray Diffraction
HR-SEM	:	High- resolution scanning electron microscopy
EDAX	:	Energy Dispersive X-Ray Analysis
XPS	:	X-ray photoelectron spectroscopy
N	:	Newton
OCP	:	Open-circuit potential
EIS	:	Electrochemical impedance spectroscopy
SBF	:	Simulated body fluid
SEM	:	Scanning electron microscopy
SPM	:	Scanning probe microscopy
GPa	:	Giga Pascal
°C	:	Degree centigrade
Ti	:	Titanium
Nb	:	Niobium
Cu	:	Copper
PM	:	Powder metallurgy
µm	:	Micrometer
BT-XRD	:	Bench top X-Ray Diffraction
RPM	:	Revolution per minute
H	:	Hour
s	:	Second
min	:	Minute
Å	:	Angstrom

°	:	Degree
Kgf	:	Kilogram force
kN	:	Kilo newton
mL	:	Milliliter
g	:	Gram
cm	:	Centimeter
Hz	:	Hertz
mV	:	Millivolt
FBS	:	Foetal bovine serum
PBS	:	Phosphate buffer saline
pH	:	Potential of Hydrogen
Ω	:	Ohm
μ A	:	Micro Ampere
eV	:	Electron volt
nm	:	Nanometer
R _a	:	Average roughness
R _q	:	Root-mean-square roughness
S _a	:	arithmetic mean height
S _q	:	squared mean height
%	:	Percentage